Development of gallium gradients in three-stage $Cu(In, Ga)Se_2$ coevaporation processes

Sebastian Schleussner, Tobias Törndahl, Margareta Linnarsson, Uwe Zimmermann, Timo Wätjen and Marika Edoff

March 17, 2011

Abstract

We use secondary-ion mass spectrometry (SIMS), X-ray diffraction (XRD) and scanning electron microscopy (SEM) to investigate the development over time of compositional gradients in $Cu(In, Ga)Se_2$ thin films grown in three-stage coevaporation processes, and suggest a comprehensive model for the formation of the well-known 'notch' structure. The model takes into account the need for compensating Cu diffusion by movement of group-III ions in order to remain on the quasi-binary tie line and indicates that the mobilities of In and Ga ions differ. Cu diffuses towards the back in the second stage and towards the front in the third, and this is the driving force for the movement of In and Ga. The [Ga]/[In + Ga] ratio then increases in the direction of the respective Cu movement because In has a higher mobility at process conditions than has Ga. Interdiffusion of In and Ga can be considerable in the $(In, Ga)_2Se_3$ film of the first stage, but seems largely to cease in CIGS and shows no signs of being boosted by the presence of a Cu_2Se layer.

1 Introduction

To date, the most successful processes for the fabrication of high-quality $Cu(In, Ga)Se_2$ for high-efficiency solar cells are the so-called three-stage process and variations of it [1, 2]. Besides their tendency to yield large-grained material with a preferred (204/220) crystal orientation, one of the most noteworthy properties of these co-evaporation processes is the double gallium gradient that they intrinsically form. An increased [Ga]/[In + Ga] ratio is reflected in the band structure as an increased level of the minimum of the conduction band, E_C. The slope in E_C induced by a gallium gradient towards the back contact has been shown by device modelling to lead to a lower saturation current and thus to a higher open-circuit voltage [3, 4]. If the diffusion length of electrons is large compared to the absorber thickness, this gain is primarily the effect of reduced recombination at the back contact. If the diffusion length is comparatively small, the more important gain from a gradient is the reduction of bulk recombination by virtue of the electrons being directed towards the junction. In the interface region, where the electron and hole concentrations n

and p are similar to each other, a larger bandgap is advantageous, since it reduces the intrinsic carrier concentration $n_i = (np)^{1/2}$ and thus the recombination rate. By not placing the minimum of the grading directly at the junction, one can therefore to some extent decouple absorption, and thus current generation, from recombination in the interface region, which influences the voltage [4]. An excessive increase of [Ga]/[In + Ga] near the front surface, however, can lead to blocking behaviour which reduces the fill factor [5]. The built-in gallium grading obtained by the standard three-stage process as described by NREL is excellent, as shown by the world-record device results, but it might still be possible to be improved. In order to control and engineer this grading, a more thorough understanding of the dependence of the gradient on the deposition parameters in the various stages is needed. Another issue is whether intentional gallium gradients can be preserved. This work investigates how the gallium is redistributed in the film during the evaporation process as a function of copper in- and out-diffusion. The information is obtained by interrupting two variations of the three-stage process, with and without a first layer where all group-III elements are replaced by only gallium. The resulting finished and non-finished films are analysed by X-ray diffraction and secondary-ion mass spectrometry.

2 Experimental

2.1 Film and device fabrication

The $Cu(In, Ga)Se_2$ and $(In, Ga)_2Se_3$ films for this study were deposited by co-evaporation of the elements Cu, In and Ga from fast-acting open boat sources in a Se atmosphere maintained from a crucible source kept at a constant temperature. The metal rates were controlled using mass-spectrometer feedback. The Se temperature was chosen such that it was safe to assume that the Se evaporation rate was several times higher than that required for the formation of stoichiometric material at all times during the process. The process was carried out in a vacuum chamber pumped to a pressure of below 2×10^{-6} mbar holding three $5 \times 5\,\mathrm{cm}^2$ substrates per run. The substrates were 1 mm thick soda-lime glass with molybdenum back contacts of 300 nm thickness deposited by DC magnetron sputtering, in accordance with our group's baseline procedure [6]. They were heated by means of a graphite susceptor with a type-K thermocouple inserted for temperature control. The relation between the susceptor temperature and the real sample temperature was determined in a calibration where a piece of glass with a Mo/CIGS coating and an embedded, very thin second thermocouple was mounted in the place of the samples. The temperature values named in this article are based on that calibration.

The upper subfigure of Figure 1 shows the rate and substrate-temperature profiles of the *reference* CIGS recipe which has a constant gallium content $x = [Ga]/[In + Ga]$ in the evaporated profiles. The lower subfigure displays the development of the *integral* film composition in the reference process over time, as calculated from the final composition and the given evaporation profiles.

The CIGS films are fabricated according to the so-called *three-stage process* [7]. This means that the evaporation of In, Ga and Se ('stage *I*') is followed by the evaporation of Cu and Se at a higher temperature, resulting in a transition to a

Cu-rich composition ('stage *II*'), and a Cu-poor composition of the final absorber film is achieved by once again evaporating the group-III elements In and Ga in a maintained Se atmosphere ('stage *III*').

Out of a total process duration of 52 min, stage *I* in our process took 15.3 min, stage *II* took 20 min, and stage *III*, 16.6 min. The substrate was kept at a temperature of 450 °C during the first stage. During the second stage this temperature was ramped up to 530 °C and it was then held at that value until the end of the evaporation. Immediately after that, the heater was turned off and the samples were left to cool in vacuum.

This reference recipe is compared with another recipe that begins with the deposition of a thin layer of indium-free gallium selenide in order to generate an intentional gallium gradient at the back. The latter recipe is illustrated in Figure 2, with the upper subfigure as before and the lower subfigure showing the resulting momentary values of the ratio x at the growth surface, calculated from the evaporation rates, in addition to the integrals calculated from the growing film as above. As shown, only gallium and selenium were evaporated during the first 2 min of stage *I* (here denoted as 'stage *I.a*'). After this point, the shutter was closed for 1.5 min to allow the indium and gallium sources to reach their new rate levels, and then the remaining 13.3 min of stage *I* were completed with the same ratio x as in the reference recipe ('stage *I.b*'). The film grown up to point *I.a* was not investigated separately, but we assume the material to exist in the same composition as the indium–gallium selenide grown otherwise, that is, as Ga_2Se_3.

In order to investigate the chronological development of gradients, we not only fabricated complete absorber layers (process ended at point '*III*') but also aborted runs of either recipe at the three points marked in Figures 1 and 2: At the end of stage *I* (point '*I*'), in the middle of stage *II* (point '*II.a*'), where the layer is Cu-poor, and at the end of stage *II* (point '*II.b*'), where the film is Cu-rich. As with the complete absorbers, the cool-down of these films started directly after the evaporation was terminated so as to maintain the structures in their as-grown states. The thicknesses and compositions of the resulting films are listed in Table 1. All samples were fabricated in separate processes, and due to small fluctuations in the mass-spectrometer sensitivity, we experience a run-to-run thickness variability of up to 10 % for the CIGS process.

Devices were finished on the samples with complete absorber films according to our previously-mentioned baseline procedure. This procedure comprised a 50-nm CdS buffer layer grown by chemical bath deposition, an RF-sputtered 50-nm layer of intrinsic ZnO, a DC-sputtered 300-nm film of Al-doped ZnO as a conductive window layer, a current-collecting Ni–Al–Ni grid and mechanical scribing to define separated 0.5 cm^2 cells.

2.2 Analyses

The final composition of the films was determined by X-ray fluorescence (XRF) performed in a *Spectro X-lab 2000* and the thickness was measured with a *Dektak V 200-Si* profilometer. For the XRF measurements to yield quantitative compositional information, the countrates were calibrated with a known reference sample according to a linear model.

Elemental depth profiles of the films were analysed by secondary ion mass spectrometry (SIMS) utilizing a *Cameca IMS 4f* instrument. A primary sputter beam of $^{133}Cs^+$ ions with an impact energy of 4.5 keV was rastered over an area of $200 \times 200\,\mu m^2$, and secondary ions of MCs^+ (M = ^{63}Cu, ^{69}Ga, ^{80}Se, ^{98}Mo or ^{115}In) were collected from a central region of ca. 60 µm diameter in the sputtered crater. The erosion rate was typically around 2 nm/s. A frequent problem in SIMS analysis is a strong matrix dependence of the ionization yield, i.e. a non-linear relation between counts and concentration. The MCs^+ complexes were used in our study in order to minimize this effect [8].

To convert the SIMS raw data to concentration-versus-depth profiles, two assumptions are made: Firstly, that the erosion rate is constant, and secondly, that the detected intensity is proportional to the concentration of the measured species. The depth scale is determined from film-thickness measurements, and the intensity-to-concentration proportionality factors are calculated from the average element content in the film as established from XRF data.

Scanning-electron microscopy (SEM) images were recorded on a *LEO 1550* microscope equipped with a field-emission electron gun and operating at an acceleration voltage of 15 kV. For cross-sectional imaging, the samples were prepared in parts like classical transmission-electron microcopy samples, with mechanical grinding being followed by ion polishing in order to reduce the final thickness of the amorphous layer on the sample surface. The cross-sectional images were acquired using a solid-state backscatter detector, the images of the SIMS crater bottoms, using an in-lens detector.

The X-ray diffraction (XRD) $\theta/2\theta$ and surface-sensitive grazing-incidence (GI-XRD) scans were performed in a *Philips X'pert MRD* equipped with an X-ray mirror and a 0.09° parallel-plate collimator, using Cu-K_α radiation in a non-focusing geometry. The angle of incidence for the GI-XRD scans was kept at 1° in order to increase the surface sensitivity of the measurement.

Cells were characterized by current-versus-voltage (IV) measurements with illumination from an ELH halogen lamp calibrated to an intensity of $100\,mW/cm^2$. The external quantum efficiency (QE) was determined under ambient lighting conditions.

3 Results and Discussion

3.1 XRD

$\theta/2\theta$ X-ray diffractograms for the reference and for the intentionally graded films are displayed in Figure 3 (a) and (b), respectively. In Figure 3 (a), the diffractograms from stages *II.a* through *III* of the reference process show only reflections from the tetragonal CIGS phase and the Mo(110) reflection. For the stage-*I* sample, all the reflections can instead be attributed to a hexagonal γ-In_2Se_3 phase [9], but are shifted towards higher angles of 2θ. The formation of a phase with γ-In_2Se_3 structure in the first stage of three-stage CIS processes was also reported by Contreras et al. [10]. Equivalently, the peaks also fit to a reported hexagonal $InGaSe_3$ phase of the same structure [11], compared to which they are shifted towards slightly lower diffracting angles. The peak shifts are probably owed to the presence of gallium

in the film, with the [Ga]/[In + Ga] ratio being below 0.5 according to XRF: In a similar manner as for the CIGS phase, a higher gallium content can be expected to make the peaks shift towards higher 2θ-values due to a smaller cell parameter.

In Figure 3 (b), the diffractograms from stages *II.a* through *III* of the process beginning with the gallium-selenide layer show the tetragonal CIGS phase as well. The only difference in phase content from the reference process is that a small reflection at $2\theta = 22.1°$ is visible in the stage *II.a* sample. Since the peak disappears during the later process stages, it may well be related to a Cu-poor phase that forms temporarily during the transformation from $(\mathrm{In,Ga})_2\mathrm{Se}_3$ to $\mathrm{Cu(In,Ga)Se}_2$ structure. The stage-*I* sample for the intentionally graded process is similar to that of the reference process, where the diffraction pattern indicates that a phase related to γ-$\mathrm{In}_2\mathrm{Se}_3$ is deposited. However, since the stage-*I* sample contains a gradient, peak broadening of reflections in the diffraction pattern occurs, which makes it more difficult to interpret than that for the reference process.

From the $\theta/2\theta$ scans in Figure 3 it can also be seen that the CIGS from the reference process is more (112)-oriented than that from the intentionally graded process, where the (220)/(204) reflections are more dominant. The CIGS peaks are asymmetric in both cases, but more so in the case of the intentionally graded samples, corroborating the SIMS results discussed below, which show that the gradient remains stronger in the latter. Comparing the diffractograms of the $(\mathrm{In,Ga})_2\mathrm{Se}_3$ precursors from stage *I*, we find that the reference precursor film exhibits a preferred (006) orientation (is *c* oriented), while the corresponding intentionally graded film is predominantly (110)/(300) oriented. This correlation between the preferred orientations of the films after stage *I* and those of the final CIGS films is in agreement with the observations of Contreras et al. [10].

Since XRF shows that the stage-*II.b* samples are Cu-rich (see Table 1), the surface layer of the stage-*II.b* and *III* samples was analysed by grazing-incidence XRD. The resulting diffractograms are shown in Figure 4. By measuring the peak position of the Mo(110) reflection, it was found that the peak shift due to the GI method was small and approximately the same for all four samples. For both stage-*II.b* samples, a small peak is found at a 2θ-value of 31.3°. This peak cannot be related to CIGS and disappears in the stage-*III* samples. Though other peaks from the cubic $\mathrm{Cu}_2\mathrm{Se}$ are difficult to observe due to their overlap with peaks from the CIGS structure, a probable explanation for this extra reflection is that it belongs to $\mathrm{Cu}_2\mathrm{Se}(200)$.

It can also be seen in the GI-XRD diffractograms that the CIGS peaks shift towards higher 2θ angles from the stage-*II.b* to the stage-*III* films, indicating that the surface regions of the latter samples contain more gallium.

3.2 SIMS and SEM

The SIMS profiles on stage-*I*, stage-*II.a* and full stage-*III* samples are uncomplicated, as exemplified by the *raw*-data profile of the full reference film in Figure 5 (a): The sputter rate appears largely constant throughout the CIGS film, and the transition into the Mo layer is relatively sharp, with an exponential decay length in the order of 25 nm on a depth scale. This decay length is several times larger than the range of 5 nm to 10 nm estimated for the broadening caused by cascade mixing

alone. Thus it is most probably the surface roughness of the samples that is the limiting factor for the depth resolution.

The measurements on the two stage-*II.b* samples, again demonstrated for the reference case in Figure 5 (b), differ markedly from the other measurements. In SEM surveys, the top surfaces of the stage-*II.b* samples do not appear rougher than those of the other samples. The transition from the CIGS into the Mo layer is much broader, though, with a decay length of about 65 nm, and furthermore, the Cu and Se signals are considerably elevated in the frontmost part, with slopes stretching over the first 300 s.

On the one hand, the signal change at the front of the stage-*II.b* samples is compatible with the detection of Cu_2Se at the surface of these samples by XRD. On the other hand, the SEM images of the bottoms of SIMS sputter craters in Figure 6 show that the sputtered surface is considerably more uneven in the stage-*II.b* sample than in the stage-*III* sample, being littered with large columns. This unevenness is also found in profilometer scans and makes the broadened transients understandable as the result of an uneven sputter front. To explain the observed effects, we first point out that Cu_2Se has earlier been found in Cu-rich samples to precipitate both on the surface and in the grain boundaries of the CIGS film [12]. Secondly, we suggest that this inhomogeneous Cu_2Se cover is eroded with a lower rate in SIMS than is the CIGS film, for in this case it will locally mask the film below for varying amounts of time and cause both the columnar residues on the crater bottom and the long decay lengths of the SIMS signal. The rise of the Cu and Se signals at the front of the stage-*II.b* sample may be explained by a higher ionization yield for these elements in a Cu_2Se matrix relative to a CIGS matrix.

These effects primarily increase the uncertainty of the depth resolution and of the Cu and Se content quantification for the stage-*II.b* samples. Even so, the standard evaluation of the data yields a Cu content very close to $y = [\mathrm{Cu}]/[\mathrm{In} + \mathrm{Ga}] = 1$ for the region not affected by the signal slopes, as is expected from the common model for Cu-rich samples where stoichiometric α-phase $\mathrm{Cu(In, Ga)Se_2}$ is capped with Cu_2Se [13]. The In and Ga signals appear to be consistent and unaffected by the Cu_2Se-induced artefacts throughout the stage-*II.b* samples. Based on these considerations, it is now possible to discuss the x profiles for all eight samples, plotted in Figure 7 as functions of the vertical position.

The SEM cross-section images of complete absorber layers depicted in Figure 8 show large grains that vertically span all or a major part of the films, and they exhibit no discernible change in grain sizes between the reference and intentionally graded samples. In particular, the gradient in the intentionally graded sample has not led to the formation of a separated layer of smaller grains at the back-contact layer. The images also demonstrate that the film surfaces are fairly even, so that the impact of as-grown surface roughness on the depth resolution of the SIMS profiles can be assumed to be limited.

3.3 Discussion

In agreement with compositional data, our X-ray diffractograms show that the films at the end of the Cu-free stage *I* consist of γ-$\mathrm{(In, Ga)_2Se_3}$. For the sample with a layer of Ga_2Se_3 deposited at the beginning, interdiffusion of In and Ga has occurred

during stage I and thus the originally ca. 130 nm thick and sharply terminated layer of Ga_2Se_3 at the back has been partly diluted, but is still relatively localized. In contrast, the reference sample with its constant deposited [Ga]/[In + Ga] ratio does not have any gradient after stage I.

In stage II, the $(In, Ga)_2Se_3$ films grown in stage I are exposed to Cu and Se. The next investigated samples are aborted at point $II.a$, where enough Cu has been added to bring the [Cu]/[In + Ga] ratio to approximately 0.6, that is to say, before the sample becomes Cu-rich relative to stoichiometric $Cu(In, Ga)Se_2$. The SIMS analyses show that gradients in the [Ga]/[In + Ga] profiles have developed by this time, with an accumulation of Ga towards the back of the film and an increased In content towards the front. This development can be explained in accordance with the fact that in-diffusion of each three Cu ions must be compensated for by out-diffusion of one group-III ion to maintain the composition on the quasi-binary tie line, with the group-III ions then able to form new unit cells on the surface together with Cu and Se atoms provided from the gas phase. In order for the [Ga]/[In + Ga] gradient to develop in the direction observed at this point in the process, out-diffusion of In has to dominate over out-diffusion of Ga, as Gabor et al. [3] noted.

At this stage, the main difference between the reference sample and the intentionally graded sample is that the sample with the gallium-selenide layer exhibits a higher gallium level towards the back, but approximately the same surface composition. In the sample with the intentional gradient, the Ga profile is more spread out and somewhat reduced in its gallium level relative to the previous point. This effect is probably owed to the lower availability of In close to the back contact, which makes it necessary for larger amounts of Ga to move towards the front in compensation for the Cu in-diffusion than is the case in the reference. Indeed, the [Cu]/[In + Ga] profiles at this point suggest that low Ga mobility may be limiting the in-diffusion of Cu in the graded sample: As seen in the [Cu]/[In + Ga] profile in Figure 7, the reference profile is constant, but the profile of the graded sample has a noticeable downward slope towards the back.

We expect the copper in-diffusion to continue until $Cu(In, Ga)Se_2$ stoichiometry is obtained, at which point practically all copper sites are filled and there is no room for additional copper in the crystal lattice, so that a copper-selenide phase starts to segregate at the surface instead. After cool-down of the samples terminated at point $II.b$, both GI-XRD and SIMS do yield evidence of copper selenide at the surface. From the SIMS profiles, we conclude that a continuous [Ga]/[In + Ga] slope towards the surface of the film has continued to develop in both samples during the Cu-poor growth stage. The higher Ga level towards the back contact in the sample with the additional gallium-selenide layer is still significant.

After the renewed addition of In and Ga in the final stage III with the same [Ga]/[In + Ga] ratio as in the end of stage I, a new gradient in the [Ga]/[In + Ga] ratio forms in both the sample with and without gallium selenide at the back, as the SIMS profiles demonstrate. This gradient is opposite to the first one and thus completes the characteristic notch profile which is commonly found after the three-stage process. The position of the minimum of the [Ga]/[In + Ga] ratio is approximately at the end of stage II, maybe slightly offset deeper into the films, and the level of the gradient at the front is not affected by the elevated Ga content in the first stage.

According to the phase diagrams published by Rau and Rabenau [14] and by Fearheiley [15], Cu_2Se can be liquid at temperatures over 523 °C in the presence of a sufficient surplus of Se. Irrespective of the actual aggregate state of this film, one may assume that when indium, gallium and selenium are added to a copper-rich sample, the CIGS grows epitaxially at the CIGS–Cu_2Se interface, as SEM cross-sections regularly indicate large grains in finished CIGS layers. Copper is readily available from the copper selenide until stoichiometry is once more reached. To achieve optimal lattice matching and minimize surface stress, the new material should thus at first preferentially grow with the same composition as the existing CIGS surface, that is to say with a slightly lower Ga content towards the CIGS surface than the In and Ga rates in the gas phase prescribe. This lattice-matching constraint would slightly favour In ions, rather than Ga ions, to react to form the chalcopyrite material, leading to a gradually increasing Ga concentration in the Cu_2Se top film. This assumed mechanism can thus be thought to prompt the formation of the first part of the opposite gradient completing the notch, although with the experiments at hand, we cannot provide direct evidence for them or quantify their contribution to the final profile.

Once the film returns to substoichiometric composition, growth must continue by means of Cu ions being withdrawn from the existing CIGS and forming new unit cells at the surface, together with In, Ga and Se atoms arriving from the gas phase. The Cu profiles in the SIMS data of the finished samples (not depicted) show a Cu depletion in about the topmost 100 nm, as found by many other studies. However, they do indicate a constant Cu concentration throughout the bulk of the film, which in turn implies that in the final section of the process, Cu moves from all of the bulk of the CIGS film towards the growth front at the surface to be included in the growing film. Following the reasoning from stage *II*, with the movement of Cu now directed outwards, diffusion of In inwards towards the back contact should now be favoured. In the bulk of the finished films, we observe a small decrease of the grading compared to the film where growth was terminated at point *II.b*, and at the front of the film the Ga concentration towards the surface is enhanced relative to the stage-*III* evaporation rates. Furthermore, the level of the reverse, stage-*III* gradient is largely unaffacted by the Ga content of the material grown in the first two stages. All these observations agree well with our view that compensation for the diffusion of Cu is the driving force for the movement of In and Ga in stages *II* and *III*, with In moving more easily than Ga and thus forming gradients.

From the large grains seen in the cross-sections in Figure 8, it seems likely that the gradients observed in the SIMS profiles mainly exist within single grains rather than being the result of a layered structure of smaller grains with differing Ga content, and that they thus primarily are affected by intragrain diffusion rather than by intergrain diffusion.

Interdiffusion between In and Ga will certainly be in effect to some degree throughout the process as a homogenizing mechanism competing with the dehomogenizing mechanisms described above. However, while we observe rather pronounced Ga–In interdiffusion between the Ga_2Se_3 and $(In,Ga)_2Se_3$ layers in stage *I*, the fact that later features are maintained fairly well suggests that the interdiffusion in our $Cu(In,Ga)Se_2$ films is not very strong. Most notable in this context is the aforementioned independence of the stage-*III* gradient from the material below it. A

similar observation was made by Chirila et al. [16], who noted that the notch profile of a film fabricated with a very fast second stage was practically identical to that of a reference film. Caballero et al. [17] report that gradients were absent in a film with a normally fast but short second stage that led to a final composition of [Cu]/[In + Ga]≈ 0.35. Taken together with our observations, this absence of gradients could mean that the elevated Ga–In interdiffusion of stage *I* is still present in the intermediate defect chalcopyrite. Contrary to what was postulated by Gabor et al. [3], we do not observe that the composition is homogenized vertically when Cu_2Se is present.

Finally, it is instructive to compare the present depth profiles to the results of an previous series [5]. In that series, the temperature during stage *I* was held at 300 °C, that is, 150 °C lower than in the current series. The gallium-enhanced layer at the back used to be followed by a layer that was indium-enhanced relative to the average gallium content; and the amount of material deposited in stage *III* was relatively speaking larger than in the current series, similar to that deposited in stage *I*.

We note that the position of the minimum of the gallium 'notch' profile in either case is close to the thickness grown in the first two stages, and that also the magnitude of the backward gradient in relation to that of the forward gradient correlates with the ratio between the stages. We also find that the intentional gradient is much less localized and pronounced now than then. This difference is probably owed to the higher temperature during the first stage which conceivably has boosted the indium–gallium interdiffusion. The form of the evaporated profiles may be an additional cause, in that the In-enhanced layer in the older series may have served as a preferred reservoir of group-III ions for compensating for the Cu in-diffusion into most of the film.

Despite the small remaining enhancement of the backward gradient, we see in Table 2 that the sample with the added gradient yields solar cells performing somewhat better than the reference. Other than the induced back-surface field, in view of various authors' findings of a beneficial (220/204) texture [18, 19], the slightly stronger (220/204) texture of the intentionally graded sample might be a cause for this difference.

4 Conclusions

We have suggested a comprehensive model explaining the development of gradients in the three-stage coevaporation of $Cu(In, Ga)Se_2$ thin films. The model combines the precondition for movement along the quasi-binary tie line with observations regarding ion mobility: When Cu diffuses into a layer of $(In, Ga)_2Se_3$, of $Cu(In, Ga)_3Se_5$, or of CIGS with a lower Cu content, one group-III (Ga or In) ion has to move into the opposite direction for every three Cu ions. This condition is relevant both in stage *II*, with Cu moving towards the back, and in stage *III*, with Cu moving towards the front. Gradients with an increasing [Ga]/[In + Ga] ratio in the direction of the respective Cu diffusion then form because In has a higher mobility at process conditions than has Ga. This assertion is made clear by the direction of the gradients and by the position of the minimum between them, and is further supported by indications that Cu diffusion is hindered when it encounters an enhanced Ga concentration. The magnitude of the gradient at the front proves

to be independent of the additional gradient at the back and thus likewise independent of the average Ga content. We therefore identify Cu diffusion, given the lower mobility of Ga compared to In, as the dominating driving force for the autonomous formation of Ga gradients in the three-stage process.

Interdiffusion of In and Ga is considerable in the Cu-free materials during stage I, at least at the fairly high stage-I temperature of 450 °C chosen in the present series. The interdiffusion might still be in effect to around the composition of $Cu(In,Ga)_3Se_5$, but seems largely to cease in CIGS and shows no signs of being boosted by the presence of a Cu_2Se layer.

Bibliography

[1] Ingrid L. Repins, Stephen Glynn, Joel Duenow, Timothy J. Coutts, Wyatt K. Metzger, and Miguel A. Contreras. Required material properties for high-efficiency CIGS modules. In Alan E. Delahoy and Louay A. Eldada, editors, *Proceedings of SPIE*, volume 7409, page 74090M. SPIE, 2009. doi:10.1117/12.828365.

[2] Michael Powalla, Georg Voorwinden, Dimitri Hariskos, Philip Jackson, and Robert Kniese. Highly efficient CIS solar cells and modules made by the coevaporation process. *Thin Solid Films*, 517(7):2111–2114, 2009. doi:10.1016/j.tsf.2008.10.126.

[3] Andrew M. Gabor, John R. Tuttle, Michael H. Bode, Amy Franz, Andrew L. Tennant, Miguel A. Contreras, Rommel Noufi, D. Garth Jensen, and Allen M. Hermann. Band-gap engineering in Cu(In,Ga)Se_2 thin films grown from $(In,Ga)_2Se_3$ precursors. *Solar Energy Materials and Solar Cells*, 41–42:247–260, 1996. doi:10.1016/0927-0248(95)00122-0.

[4] Thorsten Dullweber, Olle Lundberg, Jonas Malmström, Marika Bodegård, Lars Stolt, Uwe Rau, Hans-Werner Schock, and Jürgen H. Werner. Back surface band gap gradings in Cu(In,Ga)Se_2 solar cells. *Thin Solid Films*, 387(1–2):11–13, 2001. doi:10.1016/s0040-6090(00)01726-0.

[5] Sebastian Schleussner, Uwe Zimmermann, Timo Wätjen, Klaus Leifer, and Marika Edoff. Effect of gallium grading in Cu(In,Ga)Se_2 solar-cell absorbers produced by multi-stage coevaporation. *Solar Energy Materials and Solar Cells*, 95(2):721–726, 2011. doi:10.1016/j.solmat.2010.10.011.

[6] John Kessler, Marika Bodegård, Jonas Hedström, and Lars Stolt. Baseline Cu(In,Ga)Se_2 device production: control and statistical significance. *Solar Energy Materials and Solar Cells*, 67(1–4):67–76, 2001. doi:10.1016/s0927-0248(00)00264-6.

[7] Miguel A. Contreras, John R. Tuttle, Andrew M. Gabor, Andrew L. Tennant, Kannan Ramanathan, Sally E. Asher, Amy Franz, James C. Keane, L. Wang, John Scofield, and Rommel Noufi. High-efficiency Cu(ln,Ga)Se_2-based solar cells: Processing of novel absorber structures. In *24th IEEE Pho-*

tovoltaic Specialists Conference, pages 68–75, 1994. Available from: http://www.oberlin.edu/physics/Scofield/pdf_files/pvsc-95h.pdf.

[8] Hubert Gnaser. Improved quantification in secondary-ion mass spectrometry detecting MCs^+ molecular ions. *Journal of Vacuum Science & Technology A: Vacuum, Surfaces, and Films*, 12(2):452–456, 1994. doi:10.1116/1.579262.

[9] Anna Likforman, Daniel Carré, and Roger Hillel. Structure cristalline du séléniure d'indium In_2Se_3. *Acta Cryst. B*, 34(1):1–5, 1978. doi:10.1107/S0567740878002174.

[10] Miguel A. Contreras, Brian Egaas, David King, Amy Swartzlander, and Thorsten Dullweber. Texture manipulation of $CuInSe_2$ thin films. *Thin Solid Films*, 361–362:167–171, 2000. doi:10.1016/s0040-6090(99)00778-6.

[11] G.G. Guseinov, I.R. Amiraslanov, A.S. Kuliev, and Kh.S. Mamedov. Crystal structures of $GaInS_3$ and $GaInSe_3$. *Inorganic Materials (English translation)*, 23(5):766–768, May 1987.

[12] Jens Schöldström, Uwe Zimmermann, and Marika Edoff. Dynamic radiative properties of the Cu(In,Ga)Se_2 layer during the co-evaporation process. *Progress in Photovoltaics: Research and Applications*, 18(5):321–327, 2010. doi:10.1002/pip.931.

[13] John R. Tuttle, Miguel Contreras, Andrew L. Tennant, David S. Albin, and Rommel Noufi. High efficiency thin-film Cu(In,Ga)Se_2-based photovoltaic devices: progress towards a universal approach to absorber fabrication. In *23rd IEEE Photovoltaic Specialists Conference*, pages 415–421, May 1993. doi:10.1109/PVSC.1993.347146.

[14] Hans Rau and Albrecht Rabenau. Vapour pressure measurements in the copper-selenium system. *Journal of Solid State Chemistry*, 1(3–4):515–518, 1970. doi:10.1016/0022-4596(70)90135-0.

[15] Michael L. Fearheiley. The phase relations in the Cu,In,Se system and the growth of $CuInSe_2$ single crystals. *Solar Cells*, 16:91–100, 1986. doi:10.1016/0379-6787(86)90076-1.

[16] Adrian Chirila, Dominik Guettler, David Brémaud, Steffen Bücheler, Raineesh Verma, Sieghard Seyrling, Shiro Nishiwaki, S. Haenni, Gerhard Bilger, and Ayodhya Nath Tiwari. CIGS solar cells grown by a three-stage process with different evaporation rates. In *34th IEEE Photovoltaic Specialists Conference*, pages 000812–000816, June 2009. doi:10.1109/PVSC.2009.5411161.

[17] Raquel Caballero, Víctor Izquierdo-Roca, Xavier Fontané, Christian A. Kaufmann, Jacobo Álvarez García, Axel Eicke, Lorenzo Calvo-Barrio, Alejandro Pérez-Rodríguez, Hans-Werner Schock, and Joan Ramón Morante. Cu deficiency in multi-stage co-evaporated Cu(In,Ga)Se_2 for solar cells applications: Microstructure and Ga in-depth alloying. *Acta Materialia*, 58(9):3468–3476, 2010. doi:10.1016/j.actamat.2010.02.021.

[18] Sutichai Chaisitsak, Akira Yamada, and Akira Konagai. Preferred orientation control of $Cu(In_{1-x},Ga_x)Se_2$ ($x \approx 0.28$) thin films and its influence on solar cell characteristics. *Japanese Journal of Applied Physics*, 41(2A):507–513, 2002. doi:10.1143/JJAP.41.507.

[19] Ingrid L. Repins, Miguel A. Contreras, Brian Egaas, Clay DeHart, John Scharf, Craig L. Perkins, Bobby To, and Rommel Noufi. 19.9 %-efficient $ZnO/CdS/CuInGaSe_2$ solar cell with 81.2 % fill factor. *Progress in Photovoltaics: Research and Applications*, 16:235–239, 2008. doi:10.1002/pip.822.

5 Figures and Tables

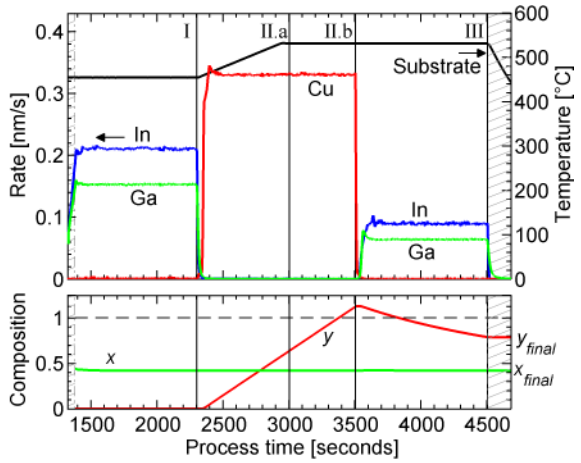

Figure 1: Top: Substrate temperature and evaporation rates of the metals Cu, In and Ga of the ungraded reference process as a function of process time. The rates are scaled data from the in-situ mass spectrometer. Bottom: Integrated composition in terms of the ratios $x = [Ga]/[In + Ga]$ and $y = [Cu]/[In + Ga]$. During segments displayed as shaded areas, a shutter is placed between the sources and the samples. Vertical lines captioned 'I', 'IIa', 'IIb' and 'III' mark points where partial processes were terminated.

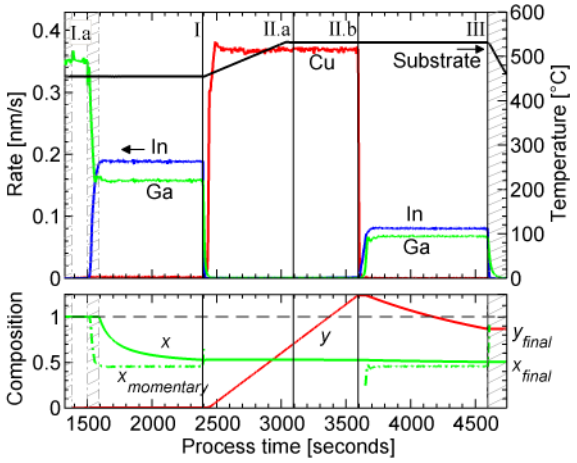

Figure 2: Top: Substrate temperature and evaporation rates of the process that includes a gallium-rich bottom layer. Bottom: Integrated composition in terms of the ratios x and y (solid lines), and the momentary x ratio (dash-dotted line). As above, the shutter was closed during the shaded segments, processes were terminated at the vertical lines.

Table 1: Characteristics for the samples discussed in this paper. Film thickness, and the final average composition in terms of $y = [\mathrm{Cu}]/[\mathrm{In} + \mathrm{Ga}]$ and $x = [\mathrm{Ga}]/[\mathrm{In} + \mathrm{Ga}]$.

Sample	thickness [µm]	y_{final}	x_{final}
reference *I*	0.90	0	0.45
reference *II.a*	1.10	0.62	0.43
reference *II.b*	1.16	1.12	0.44
reference *III*	1.80	0.79	0.42
intentionally graded *I*	1.00	0	0.51
intentionally graded *II.a*	1.26	0.63	0.50
intentionally graded *II.b*	1.26	1.18	0.51
intentionally graded *III*	1.80	0.80	0.48

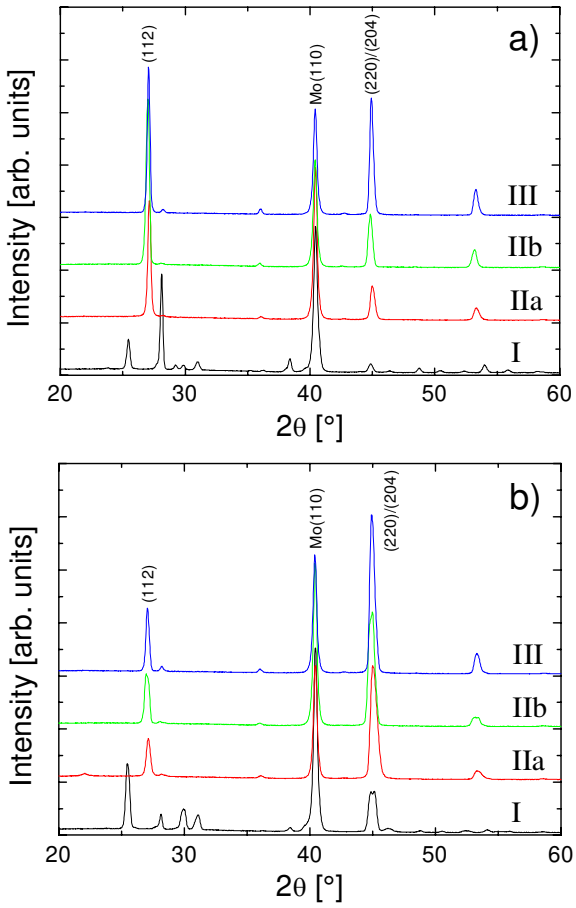

Figure 3: $\theta/2\theta$ X-ray diffractograms, measured using Cu-K_α radiation, from samples finished at points *I*, *II.a*, *II.b* and *III*. (a) Non-graded reference process and (b) process with an additional gallium-selenide layer.

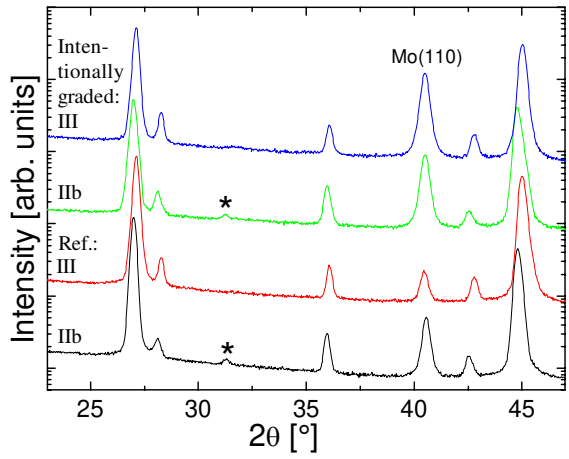

Figure 4: Grazing-incidence X-ray diffractograms from points *II.b* and *III*. The bottom two diffractograms are from the references, the top two, from the intentionally graded samples. The stars (*) at $2\theta = 31.3°$ indicate the peak position presumably belonging to the $Cu_2Se(200)$ reflection.

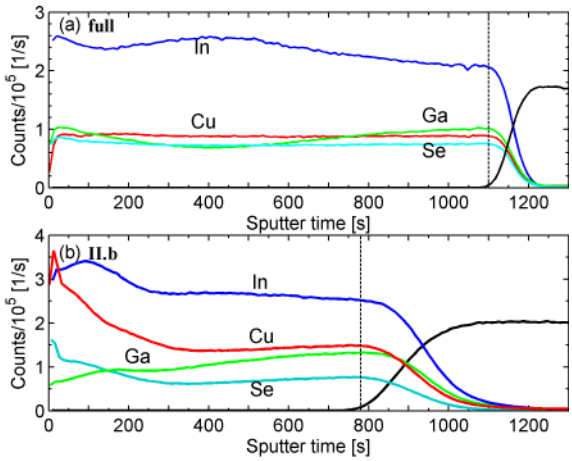

Figure 5: SIMS count-rate profiles of two reference samples: (a) full absorber (after stage *III*), (b) Cu-rich (after stage *II.b*). In case (a), the sum of the CIGS elements remains relatively constant; in case (b), the Cu and Se counts are strongly elevated at the front, and the transition from CIGS to Mo takes more than three times as much time as in (a). The dashed vertical lines demonstrate the times above which counts were considered as not belonging to the CIGS layer. Numerically, these times were defined as the points where the count sum of Cu, In, Ga and Se dropped below its thirtieth percentile, i. e. below the highest 70 % of all its values.

Table 2: Solar-cell parameters extracted from electrical measurements of the best device of either type (reference and intentionally graded): Short-circuit current density J_{SC} (verified by QE), open-circuit voltage V_{OC}, fill factor FF, efficiency η, and optical bandgap $\mathrm{E_{g,opt}}$ (according to QE); and diode parameters extracted from one-diode model fits to dark current-voltage measurements: saturation current density J_0, ideality factor n_{id}, series resistance R_{S} and shunt conductivity G_{sh}.

	reference	intentionally graded
J_{SC} [mA/cm^2]	28.1	28.8
V_{OC} [mV]	690	697
FF [%]	76.5	77.2
η [%]	14.8	15.5
$E_{\mathrm{g,opt}}$ [eV]	1.19	1.19
J_0 [mA/cm^2]	5.6×10^{-8}	4.3×10^{-8}
n_{id}	1.37	1.35
R_{S} [$\Omega\,$cm^2]	0.40	0.45
G_{sh} [mS/cm^2]	<0.1	<0.1

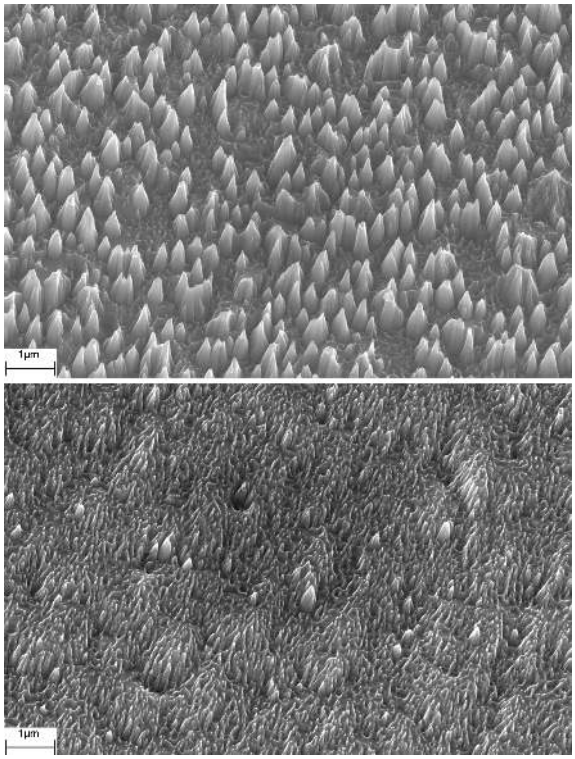

Figure 6: SEM top views of the bottoms of SIMS sputter craters on reference samples: Top, Cu-rich sample (after stage *II.b*); bottom, full absorber (after stage *III*). The images are taken at 0° of tilt; the visible slant of the structures is an effect of the oblique incidence of the sputter ions in SIMS. The larger structures in the upper image are believed to be the result of nonuniform sputtering due to an inhomogeneous Cu_2Se distribution on the original surface.

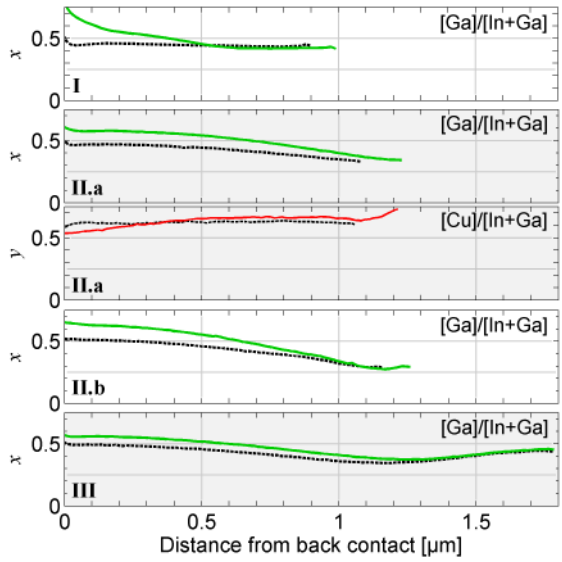

Figure 7: SIMS composition profiles of all investigated films, displayed as the ratio [Ga]/[In + Ga] over the distance from the back surface, for stage *II.a* also in terms of [Cu]/[In + Ga]. From top to bottom, stages *I*, *II.a*, *II.b* and *III*. Solid lines stand for the intentionally graded samples, dashed lines, for the references.

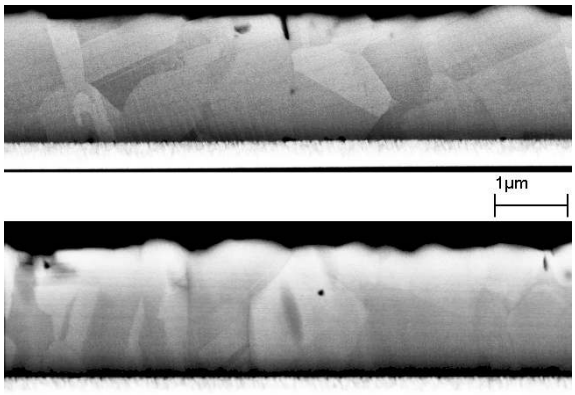

Figure 8: SEM views of polished cross-sections of full absorber layers. Top, reference sample; bottom, intentionally graded sample.